Europium Cyclooctatetraene Nanowire Carpets: A Low-dimensional, Organometallic, and Ferromagnetic Insulator

Felix Huttmann,[†] Nico Rothenbach,[‡] Stefan Kraus,[†] Katharina Ollefs,[‡] Lucas M. Arruda,[¶] Matthias Bernien,[¶] Danny Thonig,[§] Anna Delin,[§,∥,⊥] Jonas Fransson,[§] Kurt Kummer,[#] Nicholas B. Brookes,[#] Olle Eriksson,[§,@] Wolfgang Kuch,[¶] Thomas Michely,[†] and Heiko Wende[*,‡]

[†]*II. Physikalisches Institut, Universität zu Köln, Zülpicher Strasse 77, D-50937 Köln, Germany*

[‡]*Universität Duisburg-Essen and Center for Nanointegration Duisburg-Essen (CENIDE), Lotharstr. 1, D-47057 Duisburg, Germany*

[¶]*Institut für Experimentalphysik, Freie Universität Berlin, Arnimallee 14, 14195 Berlin, Germany*

[§]*Department of Physics and Astronomy, Materials Theory, Uppsala University, SE-75120 Uppsala, Sweden*

[∥]*Department of Applied Physics, School of Engineering Sciences, KTH Royal Institute of Technology, Electrum 229, SE-16440 Kista, Sweden*

[⊥]*SeRC (Swedish e-Science Research Center), KTH Royal Institute of Technology, SE-10044 Stockholm, Sweden*

[#]*European Synchrotron Radiation Facility, 71 Avenue des Martyrs, CS40220, F-38043 Grenoble Cedex 9, France*

[@]*School of Science and Technology, Örebro University, SE-701 82 Örebro, Sweden*

E-mail: heiko.wende@uni-due.de

We investigate the magnetic and electronic properties of europium cyclooctatetraene nanowires (EuCot) by means of low-temperature x-ray magnetic circular dichroism (XMCD) and scanning tunneling microscopy (STM) and spectroscopy (STS). The EuCot nanowires are prepared *in situ* on a graphene surface. STS measurements identify EuCot as a wide-band-gap semiconductor with a band gap of 2.3 eV. By means of Eu $M_{5,4}$ edge XMCD, orbital and spin magnetic moments of $(-0.1 \pm 0.3)\,\mu_B$ and $(+7.0 \pm 0.6)\,\mu_B$, respectively, were determined. Field-dependent measurements of the XMCD signal at the Eu M_5 edge show hysteresis for grazing x-ray incidence at 5 K, thus confirming EuCot as a ferromagnetic material. Our density functional theory calculations reproduce the experimentally observed bandgap. Modelling the experimental results theoretically, we find that the effective interatomic exchange interaction between Eu atoms is of the order of meV, that magnetocrystalline anisotropy energy is roughly half as big and that dipolar energy is approximately ten times lower.

Graphical TOC Entry

TOC ENTRY REQUIRED

Sandwich molecular wires (SMWs) are a particular one-dimensional class of organometallic structures, distinct from zero-dimenensional molecular magnets,[1,2] two-dimensional organometallic networks[3–5] and molecular magnetic hybrid structures on surfaces.[6,7] They consist of a periodic sequence of $4f$ rare-earth metal cations, predominantly ionically bound and eightfold coordinated to planar aromatic anions, based on the cyclooctatetraene (C_8H_8, briefly Cot) molecule as ligand.[8] Due to organometallic hybridization between the metal atomic states and the extended π orbitals of the Cot, the metal ions in the wire were proposed to couple magnetically.[9] These systems could be more stable magnetic units than single-molecule magnets, and could display larger magnetic anisotropy with correspondingly higher blocking temperatures.

A prime example is the EuCot SMW, for which chain lengths of up to 30 formula units could be achieved by Hosoya et al. through gas phase synthesis.[10] Liquid phase synthesis was realized by Tsuji et al,[11] though the product was contaminated with ferromagnetic EuO, making the interpretation of its magnetic properties problematic. Recently some of us introduced an on-surface synthesis method for EuCot, which operates under ultra-high vacuum conditions and yields a clean, phase-pure product with wire lengths up to 1000 formula units.[12]

In Stern-Gerlach type experiments by Miyajima et al.[13] the magnetic moment of EuCot was found to increase linearly with chain length and to be consistent with $m = 7\,\mu_B$ for each Eu ion, as expected for Eu^{2+}. Though experiments up to now could not make a statement on the presence of magnetic coupling between the paramagnetic Eu^{2+} ions in EuCot, in density functional theory (DFT) calculations a ferromagnetic coupling of the Eu^{2+} ions with $m = 7\,\mu_B$ is invariably found.[9,14–16] For the infinite wire, the ferromagnetic state is favored over the antiferromagnetic state by 2.5 meV according to Atodiresei et al.,[9] by 6 meV in the calculations of Xu et al.,[15] and by 1.2 meV in theoretical work of Yao et al.[16] EuCot is semiconducting with electronic band gaps of 2.0 eV

resp. 1.92 eV for the majority channel and of 3.1 eV resp. 2.94 eV for the minority channel as found in the DFT calculations of Xu et al.[15] resp. Yao et al.[16] Furthermore, EuCot wires suspended between Au electrodes were proposed to be nearly perfect spin filters by Xu et al.[15]

Based on the new on-surface synthesis method for EuCot, in this contribution we investigate the magnetic and electronic properties of EuCot SMWs experimentally by using element-specific low-temperature x-ray magnetic circular dichroism (XMCD) experiments and scanning tunneling spectroscopy (STS). We experimentally confirm the theoretical proposition of EuCot being a ferromagnetic semiconductor. At 5 K we find an open hysteresis loop for magnetization along the wire axis and considerable magnetic anisotropy by angular- and field-dependent XMCD investigations.

Scanning tunneling microscopy (STM), STS, and low-energy electron diffraction (LEED) measurements were conducted in the STM lab in Cologne, while x-ray absorption spectroscopy (XAS) and XMCD measurements complemented by sample characterization with STM and micro-channel plate (MCP) LEED were conducted at the high-field-magnet end station of the ID32 beamline of the European Synchrotron Radiation Facility (ESRF).

Prior to each experiment, the Ir(111) sample was prepared by cycles of noble gas sputtering (Xe or Ar), flash annealing to 1500 K (Cologne) or 1670 K (ESRF). At the ESRF, initial oxygen firing at temperatures up to 1670 K was applied, too. A fully closed, well-oriented layer graphene (Gr) was prepared by room-temperature ethylene adsorption until saturation, thermal decomposition at 1470 K and subsequent high-temperature exposure at 1270 K to 1×10^{-6} mbar ethylene.[17] The same quality Gr sheet was realized at the ESRF through exposure to 1×10^{-6} mbar ethylene for 600 s at a sample temperature of 1500 K. The orientation and closure of the Gr layer was confirmed in both labs through LEED and STM. A 60 % coverage of Gr/Ir(111) with EuCot nanowire islands of single-layer height was realized by simultaneous room-temperature exposure to a pressure of 5×10^{-7} mbar Cot molecules and a flux of 1.9×10^{16} s^{-1} m^{-2} Eu atoms for 105 s. Cot molecules were admitted through a gas dosing valve and Eu was sublimated from a water-cooled Knudsen cell.

The magnetic properties of the Eu ions, in the EuCot nanowires, were investigated by means of XAS- and XMCD-measurements. The data were taken in drain current mode using fully (100 %) circularly polarized light. The magnetic field of up to 9 T was aligned either parallel or antiparallel to the incident x-ray beam. By rotating the sample around the vertical axis we could adjust the angle θ of the incident x-rays to the surface normal between normal incidence (θ=0^o) and grazing incidence (θ=60^o). Hence, we have been able to obtain information about the magnetic anisotropy of the nanowires. The sample can reach temperatures down to ∼5 K and can go up to ∼325 K. To avoid nonmagnetic artifacts due to switching either the magnetic field or the polarization of the x-rays, all magnetic measurements have been done for all four combinations of field direction and polarization. In order to minimize radiation damage of the EuCot wires, we applied settings of the mirrors that yield a defocusing of 1 mm in vertical direction, while the beam size in horizontal direction was about 100 μm. Using these settings, subsequently recorded XAS and field-dependent XMCD magnetization curves did not show significant changes with time. We performed the magnetic measurements on several identically prepared samples to ensure that the total exposition time of our samples to the x-rays is minimized.

The electronic structure calculations employed the full-potential linear muffin-tin RSPt code.[18] The calculations made use of the generalized gradient approximation and the basis set consisted of *spd* basis functions while the $4f$ states were treated as non-hybridizing core states. The $4f$ shell was allowed to spin-polarize forming a net spin moment of 7 μ_B, while the orbital moment in accordance to Russel-Saunders coupling is zero. The polarization of the $4f$ shell induced a spin-polarization also of the itinerant valence electrons, via the

exchange-correlation functional. The calculations ignored the influence of the substrate and focused only on the free EuCot molecule. Also, the first principles calculations were performed only for the electronic structure, magnetic moments and valence stability.

The thermal ground state of atomistic spins $\{\vec{m}_i\} = m_i\{\vec{e}_i\}$ at site i in the Eu wire is obtained from energy minimization by Monte Carlo simulations on the Metropolis algorithm.[19] The Hamiltonian is

$$\mathcal{H} = -\sum_{<i,j>} J\vec{m}_i \cdot \vec{m}_j - \sum_{ij} \vec{m}_i \mathbf{Q}_{ij} \vec{m}_j + K\sum_i (\vec{m}_i \cdot \hat{e})^2 - \mu_B \vec{B} \sum_i \vec{m}_i, \qquad (1)$$

consisting of Heisenberg interaction between nearest-neighbor spins of strength J, dipole-dipole interaction via the dipolar tensor $\mathbf{Q}_{ij}$ in the point-dipol approximation,[20] uniaxial magnetocrystaline anisotropy and Zeeman term, respectively. K is the anisotropy constant and $\vec{B}$ the external magnetic field.

With knowledge about the exchange couplings J, one can estimate the phase transition temperature T_C from mean field theory via $k_B T_C^{MF} = 32 \sum_j J_{0j}$ or from Monte Carlo simulations via both the susceptibility χ and Binder's fourth cumulant[19] for different simulated system sizes. By definition,[21] the phase transition temperature T_C is determined only from interaction terms in Eq. (1); K and B are zero. By varying B along the wire, we obtain hystereses loops, where the coercive field B^{coer} is extracted from an interpolation of the average magnetization as a function of the external magnetic field $M(B)$ and $M(B^{coer}) = 0$. The Monte Carlo simulations were performed using the UppASD software.[22,23]

We simulate a repetition (10 times) of a Eu wire consisting of 1000 atoms without periodic boundary condition to form a carpet. To reduce thermal noise we account for 15 replica of this setup. It turned out that this size is still to small to see domain wall nucleation, although it is allowed by the model in Eq. (1). The easy axis $\vec{e}$ is in-plane and along the wires. J, K as well as temperature T are parameters of our study. Note that the nearest neighbor interaction J is only along the wire; direct exchange between the wires is set to zero.

Fig. 1 depicts the structure of the EuCot nanowire film investigated by STS, XAS, and XMCD. As visible in Fig. 1(a), the film with a coverage of 0.6 ML is formed. The analysis shows that the islands are (6.1 ± 0.5) Å high with straight edges that consist of parallel nanowires. The islands are distributed in almost random orientation on Gr/Ir(111). Each wire is composed of an alternating sequence of Eu^{2+} cations and Cot^{2-} anions [compare Fig. 1(b)].[10,24] Each Eu^{2+} is eightfold coordinated (hapticity $\eta = 8$) to neighboring Cot^{2-}. Based on STM and LEED, we find primitive translations of the wire carpet unit cell (light blue in the inset of Fig. 1(a) and in Fig. 1(c)) of 4.4 Å and 7.15 Å. These values correspond to an intra-wire separation of 4.4 Å and an inter-wire separation of 6.8 Å . The 42 eV MCP-LEED pattern in Fig. 1(d) displays first-order moiré reflections around the (0,0) spot and two concentric diffraction rings characteristic for the EuCot primitive translations defined by the EuCot carpets and consistent with a close-to random orientation distribution of the EuCot islands. A slight preference for island orientations along $\langle 1\bar{1}0\rangle$ and $\langle 11\bar{2}\rangle$ is visible in the MCP-LEED pattern through intensity variations of the diffraction rings. Due to the low electron beam currents, the EuCot MCP-LEED patterns were stable on the time scale of 1000 s and did not show degradation, while the EuCot reflections faded away on the time scale of 100 s in standard LEED.

We now turn to the discussion of the XAS and XMCD spectra. Since the magnetism of Eu originates from the $4f$ electrons, we investigate the Eu $M_{5,4}$ edges, i.e., transitions from initial $3d_{5/2}$ and $3d_{3/2}$ to the final $4f$ states. Fig. 2(a) shows the XAS signal across these edges for a 0.6 ML EuCot coverage on Gr/Ir(111). The measurements were performed at a sample temperature of $T = 5$ K and an external magnetic field of $B = 9$ T with left (μ^-) and right (μ^+) circularly polarized x-rays at grazing incidence ($\theta = 60^o$) with respect to the sample surface. The spectra are presented on a vertical scale

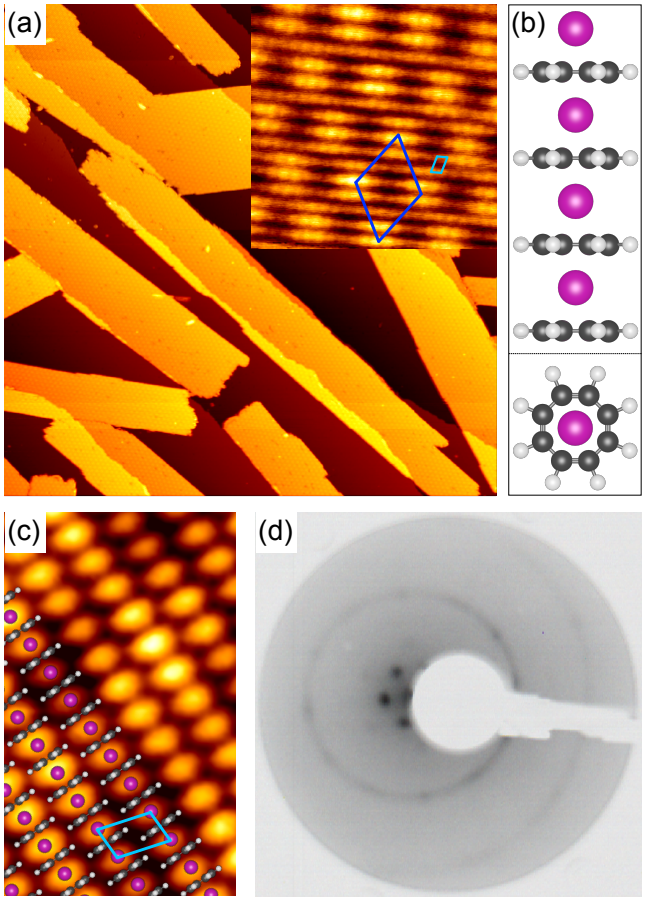

Figure 1: (a) STM topograph of a 0.6 ML EuCot nanowire film on graphene on Ir(111). Image size $260 \times 260\,\mathrm{nm}^2$, tunneling voltage $U = -3.0\,\mathrm{V}$, tunneling current $I = 52\,\mathrm{pA}$. In the inset the wire structure can be identified clearly. The unit cell of the wire carpet is indicated as light blue rhomboid. Hexagonal pattern of height modulations is due to the Gr/Ir(111) moiré. The moiré unit cell is indicated as a dark blue rhombus and has an edge length of 2.53 nm. Image size $10 \times 10\,\mathrm{nm}^2$, $U = -3.0\,\mathrm{V}$, $I = 58\,\mathrm{pA}$. (b) Side view and view along the wire axis of the DFT-based structure model[12] (Eu pink, C dark grey, H light grey). (c) High-resolution topograph of EuCot, partially overlaid with a structural model and indicating experimentally measured geometry. The light blue rhombus indicates the wire carpet unit cell. Image size $5 \times 3\,\mathrm{nm}^2$, $U = -3.1\,\mathrm{V}$, $I = 60\,\mathrm{pA}$. (d) 42 eV micro-channel plate LEED pattern of 0.6 ML EuCot film on Gr/Ir(111) after the film was used for the field-dependent XMCD magnetization curve measurements shown in Fig. 3. Two diffraction rings due to EuCot islands and moiré reflections around the (0,0)-spot are present.

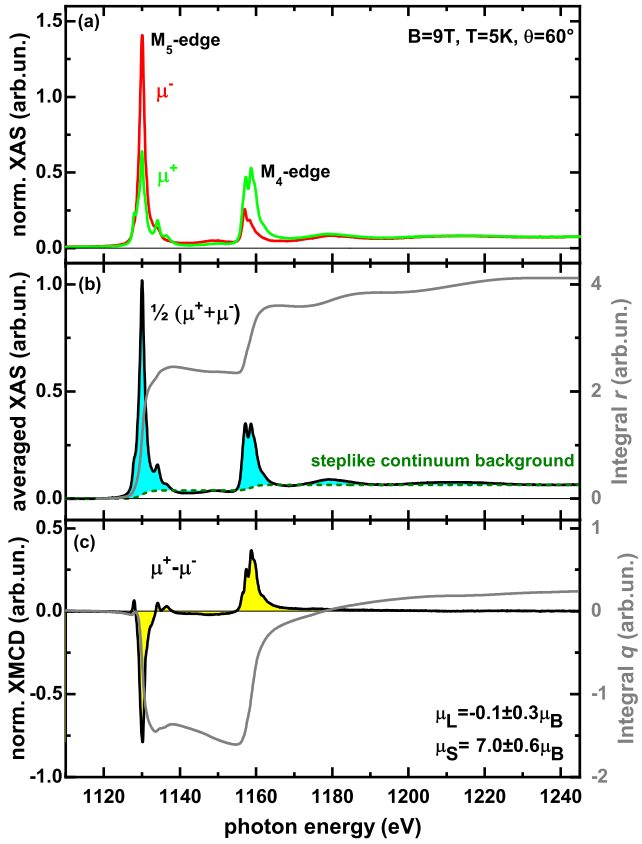

Figure 2: (a) XAS of the Eu M_5 and M_4 edges measured at grazing incidence with $\theta = 60°$, $T = 5\,\mathrm{K}$, $B = 9\,\mathrm{T}$, and with left (μ^-) (red solid line) and right (μ^+) (green solid line) circularly polarized x-rays. (b) Polarization-averaged XAS $12(\mu^+ + \mu^-)$ (black solid line) with a step function (green dashed line) used to separate the $M_{5,4}$ contributions (blue area) from the continuum. Also indicated is the integrated XAS (grey line, right y axis) after background subtraction. (c) Normalized XMCD $(\mu^+ - \mu^-)$ (black solid line and yellow area) and integral XMCD (grey line, right y axis).

that has been adjusted to zero in the pre-edge region and to one at the peak maximum of the averaged XAS. In these units, a constant value of 1.7 arb.un. corresponding to the pre-edge intensity has been subtracted from all the spectra.

Fig. 2(b) shows the polarization-averaged XAS $12(\mu^+ + \mu^-)$ with a steplike continuum background. The lineshape of the Eu $M_{5,4}$ edge XAS displays clearly divalent Eu^{2+}.[25–27] Therefore, we exclude different integer oxidation states. The 3 : 2 ratio of the step heights (branching ratio) at the M_5 and M_4 edges results from the degeneracy of the $3d_{5/2}$ and $3d_{3/2}$ orbitals. This is in agreement with Eu XAS analysis in literature.[27–29] By subtracting the continuum background we separate the $M_{5,4}$ contributions (blue area) from the averaged XAS. The integral r [Fig. 2(b), right axis] of the $M_{5,4}$ contributions is used for normalization in the sum rule analysis.

Fig. 2(c) displays the XMCD signal $(\mu^+ - \mu^-)$ which results from the subtraction of the two absorption spectra with positive and negative helicity. By applying sum rule analysis to the XMCD data we can approximate the orbital (μ_L) and spin (μ_S) magnetic moments:[28,30]

$$\mu_l = -n_h \frac{q}{r} \mu_B \,, \tag{2}$$

$$\mu_S = -n_h \frac{5p - 3q}{2r} \mu_B - 6 \langle T_z \rangle \mu_B \approx -n_h \frac{5p - 3q}{2r} \mu_B, \tag{3}$$

where the values p and q [Fig. 2(c), right axis] describe the integrals of the XMCD over the M_5 and $M_{5,4}$ edges, respectively, n_h identifies the number of holes in the $4f$ shell (here $n_h = 7$) and r is the integral of the averaged XAS, mentioned above. We approximated the dipolar term $\langle T_z \rangle$ as zero corresponding to the atomic properties of Eu^{2+} in $4f^7$ configuration.

Applying sum rule analysis, we confirm the orbital moment μ_L to be zero within the error bar of our measurements, i.e. $\mu_L = (-0.1 \pm 0.3)\,\mu_B$, but also allows the interpretation of a small but finite value. For the spin moment μ_S we obtain $\mu_S = (+7.0 \pm 0.6)\,\mu_B$, which is in good agreement with the expectation from the atomic properties of $+7.0\,\mu_B$. We note: (1) The measured magnetic moments of the Eu ion display, strictly speaking, only the time-averaged projection of the moments along the x-ray direction. We are confident that, for a sample temperature of 5 K, we are in the vicinity of saturation. Thus, we rule out temperature-dependent fluctuations of the calculated magnetic moment and equate them with the true saturated values. (2) Applying the sum rules for rare earths is challenging, in particular due to the uncertainties of the separation of the absorption edges and the long-range magnetic background. For more information on the origin of the errors in the sum rule analysis, see the supplementary information. In good approximation, the calculated values from the sum rule analysis imply that Eu is present in the half-filled $4f^7$ configuration as in its bulk state. This is in agreement with the divalent Eu^{2+}-state that we derived from the spectral lineshape of the averaged XAS.

In addition we performed XAS and XMCD measurements in a magnetic field of $B = 9\,\mathrm{T}$ for sample temperatures of $T = 7\,\mathrm{K}$ and $T = 10\,\mathrm{K}$, which results in a slightly reduced magnetization by 9 % and 10 %, respectively, as compared to the value at 5 K. This reduction of μ_S is attributed to the ensuing increased spin fluctuations with increasing temperature. For more details on the temperature dependent XAS measurements, see the supplementary information.

To investigate magnetic coupling and anisotropy of the system, in Fig. 3 we plot the field-dependent XMCD signal at the M_5 edge normalized to the pre-edge value in dependence of the magnetic field. We assume the Eu magnetization to be proportional to the XMCD signal. The magnetization is given in arbitrary units scaled to a value of 1.0 at $B = 9\,\mathrm{T}$. While Fig. 3(a) measured at the lowest attainable temperature of 5 K and normal incidence ($\theta = 0°$) displays no loop opening, Fig. 3(b) recorded at the same temperature and grazing incidence with $\theta = 60°$ shows a clear hysteresis with a coercive field of 0.2 T [compare inset of Fig. 3(b)]. We note that measuring the in-plane magnetization displays an

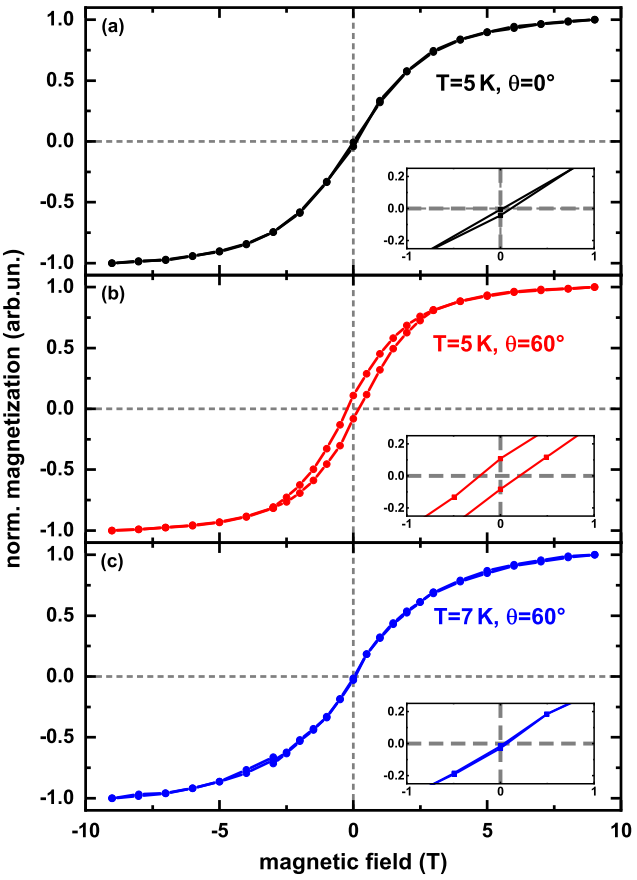

Figure 3: Field-dependent XMCD signal at the Eu M_5 edge ($E_{hv} = 1130.1\,\mathrm{eV}$) for $-9\,\mathrm{T} \leq B \leq 9\,\mathrm{T}$, normalized such that the field-dependent XMCD signal at $B = 9\,\mathrm{T}$ is 1.0. Insets magnify the magnetization in the range $-1\,\mathrm{T} \leq B \leq 1\,\mathrm{T}$. (a) Magnetization for normal incidence with $\theta = 0°$ at 5 K. (b) Magnetization for grazing incidence with $\theta = 60°$ at 5 K. (c) Magnetization for grazing incidence with $\theta = 60°$ at 7 K.

average of the spectra for the entire EuCot nanowire film, which consists of randomly oriented islands, and therefore is an average of the contributions along the wires and perpendicular to them, in the surface plane. Hence, the resulting coercive field is much smaller than the value of 2.5 T where the magnetization curve closes. After observing an open loop at 5 K, we measured field-dependent XMCD signals at the Eu M_5 edge for successively 10 K and 7 K, to assess the Curie temperature T_C of the EuCot wire carpets. At 10 K and 7 K no open loop is observed. Fig. 3(c) displays exemplarily the 7 K-measurement. After cooling down to 5 K the loop re-opens again. Hence, the Curie temperature T_C lies between 5 K and 7 K. These observations are interpreted as clear indications for ferromagnetic coupling of the EuCot nanowire carpet, with the easy magnetization direction in the surface plane.

We would like to note that we cannot specify the exact role of graphene on the magnetic anisotropy, since we cannot prepare the EuCot-wires without the graphene substrate. Hence we can not perform a similar study like e.g. shown in Lisi *et al.*[31] , where the anisotropy of the orbital moment of a two-dimensional iron phthalocyanine (FePc) network was compared to a thick FePc film without graphene as a reference. However, such a thick reference film does not exist in our case. Therefore, we cannot identify the influence of graphene on the magnetic anisotropy.

Previous calculations[9] gave the single-ion anisotropy of Eu in EuCot to be on the order of only a few eV, consistent with our own DFT calculations. However, as will be discussed below, a much higher magnetocrystalline anisotropy of about 0.5 meV has to be present to explain the experimental observations. In contrast, the anisotropy energy resulting from the magnetic dipolar interaction is on the order of 100 eV due to the large moment of 7 μ_B, and, according to these calculations, would thus entirely dominate the magnetic anisotropy. More precisely, we have calculated the dipolar energy for three different orientations of magnetic moments in the EuCot nanowire carpet: (a) along the wire axis, $E_a = -0.0745\,\mathrm{meV}$; (b) perpen-

dicular to wire axis, but in the plane of the carpet, $E_b = -0.0050\,\text{meV}$; and (c) perpendicular to the plane of the carpet, $E_c = +0.0795\,\text{meV}$.

This means, for normal x-ray incidence all wires are magnetized in a hard direction – explaining the absence of hysteresis – while for grazing incidence, despite the random in-plane orientation of the wires, for some EuCot islands a large component of the applied magnetic field is along the easy axis. In this view, the moderate susceptibility at grazing x-ray incidence is tentatively assumed to result from the difficulty to orient the magnetic moments in EuCot wire islands that are substantially misoriented with respect to the projection of the magnetic field onto the sample plane.

We also considered alternative explanations for the magnetization loop opening that can be excluded as explained in the following: 1) One might speculate that ferromagnetic EuO has formed, during growth or later by oxidation from the residual gas, which certainly would give rise to a loop opening. However, (i) EuCot synthesis is efficient and performed in large Cot excess, such that we never observed any sign of metallic Eu on the sample with STM after EuCot growth, which also rules out EuO formation during subsequent treatment. Moreover, (ii) EuO is magnetically soft, with a coercive field of less than 100 mT,[32] and thus cannot be responsible for an opening persisting up to 2.5 T. In addition, (iii) EuO has a $T_C = 69\,\text{K}$, inconsistent with our finding of $T_C \leq 7\,\text{K}$. 2) We considered that a layer of intercalated Eu under Gr could have accidentally formed, which would be strongly ferromagnetically coupled. However, as mentioned already above, (i) with STM we never observed any sign of metallic Eu, be it adsorbed or intercalated, on the sample after EuCot growth. Moreover, (ii) intercalated Eu is magnetically soft as well, as discussed in Ref. 27. The large coercive field can then only be explained by a strong in-plane uniaxial anisotropy, and Eu in EuCot islands is the only possible explanation. Consistent with the magnetic loop opening due to the presence of Eu in EuCot is the fact that the loop opening is subject to x-ray radiation damage when the sample is intentionally illuminated with higher x-ray flux, as typical for an organometallic system. For more details on the effect of radiation damage on the magnetization curves, see the supplementary information.

Figure 4: (a) dI/dV point spectrum on a EuCot island. The tip was stabilized at $U = -1.0\,\text{V}$ and $I = 5\,\text{nA}$ prior to feedback loop opening. The spectrum displayed is the average over 5 subsequent spectra with the same tip at the same location of an EuCot island indicated by the blue dot in the STM topograph shown as inset. Image size $25\times 100\,\text{nm}$, $U = -2.0\,\text{V}$, $I = 66\,\text{pA}$. Thin vertical lines indicate positions where the dI/dV signal raises over the noise level in the tunneling gap. (b) The projected density of states for Eu $5d$ and C $2p$ orbitals for spin up (positive) and spin down (negative).

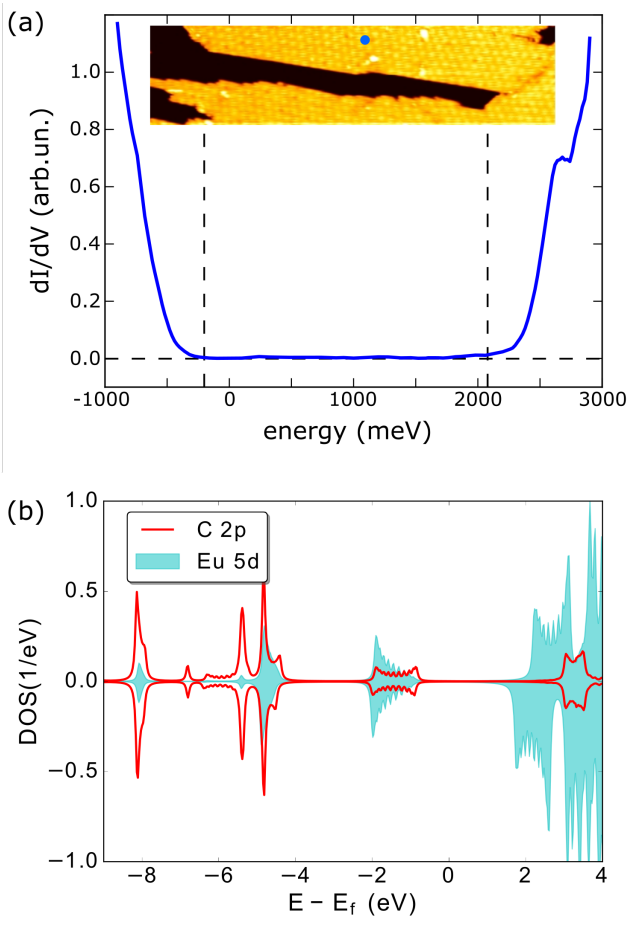

Fig. 4 provides further insight into the electronic structure of the EuCot nanowires. In Fig. 4(a) a typical STS point spectrum taken on a monolayer thick EuCot island is provided (see inset for location of spectroscopy). From the

spectrum it is obvious that the EuCot wires are wide band gap semiconductors. The electronic band gap is estimated to 2.3 eV and ranges between -0.2 eV and 2.1 eV. For this estimate the band edges were identified as the locations where the dI/dV intensity moves just out of the noise level within the gap. Note that due to their localized nature, the Eu $4f$ states are not expected to contribute to the tunneling current. They are therefore invisible in STM and may be located within the gap as measured by STS. Therefore the measured band gap corresponds to the minority bandgap and is considerably smaller than the ≈ 3 eV calculated before.[15,16]

The spin components of the density of states (DOS) resulting from our DFT calculations are shown in Fig. 4(b). As can be seen, the system is an insulator with a band gap of about 2.1 eV, which agrees rather well with the experimentally observed gap. The bandgap is determined for our case by the minority channel. In Fig. 4(b) we only show the dominant parts of the atom and l-projected DOS curves, i.e. the C $2p$ and Eu $5d$ states. Note that since the $4f$ electrons are localized, we have excluded them from the graph. However, the 4f electron states may come into play for excitation energies of around 2 eV, since the energy difference between the di- and trivalent state is about 2 eV. We conclude this based on the Born-Haber analysis presented in the supplementary information. To be precise, the valences of a bare Eu wire and a EuCot wire are calculated to be divalent, with an energy gap to the trivalent configuration of 1.94 eV respectively 2.08 eV.

Fig. 4(b) shows that there is a significant hybridization between C 2p and Eu 5d states, especially for the occupied states. This shows up most markedly from peaks that have common large intensity of both types of orbitals. The exchange splitting is largest for Eu 5d states, which is most noticeable for the unoccupied states. This exchange splitting is induced by the exchange and correlation from the large spin density of the $4f$ shell, which has a net moment of $7\,\mu_B$. The induced exchange splitting of the 5d states is found also for the occupied states, and for this reason a small moment of $0.05\,\mu_B$ emerges on the Eu valence states (excluding the $7\,\mu_B$ of the $4f$ shell). We note here that in this kind of calculations there is also an interstitial contribution to the moment, located between the Eu atom and the Cot molecule, that has an induced magnetization that is difficult to assign to a specific atom or orbital angular momentum state. The net induced moment, summed over interstitial contribution and all atom and angular momentum projected states, is, however, vanishing, since the induced moment of $0.05\,\mu_B$ on Eu states is compensated exactly by the induced interstitial moment and the moment projected on the Cot molecule. This results in a calculated moment of $7\,\mu_B$/f.u.. An integer value of the magnetic moment is a natural outcome of any magnetic insulator, since an integer number of bands of the spin-up and spin-down states are occupied.

A theoretical analysis of the dependence of the coercive field with respect to temperature finds that the coercive field decays very fast with respect to temperature, and vanishes close to the ordering temperature (compare supplementary information). This is in agreement with our observations. The Monte Carlo simulations with an exchange coupling of 1.2 meV matched to the experimental $T_C \approx 6$ K enable us to conclude that in addition to the dipolar anisotropy of about 0.15 meV an additional and even larger magnetic anisotropy of about 0.5 meV has to be present in order to reproduce the experimentally observed coercive field of 0.2 T. Previous[9] DFT calculations yielded magnetocrystalline anisotropies of the order of $5\,\mu$eV. We note that the determination of the magnetocrystalline anisotropy energies is very challenging because of the smallness of the values, and we have not attempted to explain the estimated magnetic anisotropy from the DFT calculations. Furthermore, we cannot exclude the presence of other anisotropies in the system, e.g. symmetric anisotropy exchange,[33] that are not included in our model, or effects stemming from the influence of the substrate.

Concluding, we have shown experimentally through a combination of XMCD and STS that EuCot is a ferromagnetic insulator. The size

of the bandgap from experiment is well reproduced by density functional theory calculations. We have analyzed the measured results using an effective spin-Hamiltonian that contains interatomic exchange, dipolar energies, magnetic anisotropy and a Zeeman term. Measurements are reproduced from a model where the interatomic exchange is of order meV, the magnetic anisotropy is roughly half of the exchange and dipolar energy is roughly one order of magnitude smaller that the exchange interaction. We are confident that the finding of ferromagnetic ordering in an experimentally well-accessible, surface-supported, organometallic system will provide new inspiration to the field of molecular spintronics.

Acknowledgement We are grateful to Samara Keshavarz for performimg the DFT calculation and to Dr. Yaroslav Kvashnin for valuable discussions. We thank the European Synchrotron Radiation Facility (ESRF) for beamtime allocation (experiment HC-2698) and the beamline ID32 staff for the kind support. O.E. acknowledges support from eSSENCE, the Swedish Research Council, the KAW foundation (projects 2013.0020 and 2012.0031) and the Foundation for Strategic Research. H.W. and T.M acknowledge support from DFG through projects WE 2623/17-1, and MI 581/23-1. H.W. and N.R. acknowledge funding by the Deutsche Forschungsgemeinschaft (DFG, German Research Foundation) - Projektnummer 278162697 - SFB 1242. S.K. and F.H. acknowledge financial support through the Institutional Strategy of the University of Cologne within the German Excellence Initiative. L.M.A., M.B. and W.K. thank the BMBF for financial support (no. 05K13KEA "VEKMAG"). L.M.A. acknowledges CAPES for funding (no. 9469/13-3).

Supporting Information Available

Supporting information on the experimental results, including detailed information on the sum-rule analysis, the temperature dependence and the effect of radiation damage to the absorption spectra and the field-dependent measurements is given. Moreover, supporting information to the theoretical results, including the determination of the valence stability and the finite temperature effects of the coercive field is provided.

References

(1) Sanvito, S. Molecular spintronics. *Chem. Soc. Rev.* **2011**, *40*, 3336–3355.

(2) Cinchetti, M.; Heimer, K.; Wüstenberg, J.-P.; Andreyev, O.; Bauer, M.; Lach, S.; Ziegler, C.; Gao, Y.; Aeschlimann, M. Determination of spin injection and transport in a ferromagnet/organic semiconductor heterojunction by two-photon photoemission. *Nature Mater.* **2009**, *8*, 115.

(3) Barth, J. Fresh perspectives for surface coordination chemistry. *Surface Science* **2009**, *603*, 1533.

(4) Gambardella, P.; Stepanow, S.; Dmitriev, A.; Honolka, J.; de Groot, F.; Lingenfelder, M.; Gupta, S.; Sarma, D.; Bencok, P.; Stanescu, S. et al. Supramolecular control of the magnetic anisotropy in two-dimensional high-spin Fe arrays at a metal interface. *Nat. Mater.* **2009**, *8*, 189–193.

(5) Wäckerlin, C.; Nowakowski, J.; Liu, S.; Jaggi, M.; Siewert, D.; Girovsky, J.; Shchyrba, A.; Hählen, T.; Kleibert, A.; Oppeneer, P. et al. Two-Dimensional Supramolecular Electron Spin Arrays. *Adv. Mater.* **2013**, *25*, 2404–2408.

(6) Wende, H.; Bernien, M.; Luo, J.; Sorg, C.; Ponpandian, N.; Kurde, J.; Miguel, J.; Piantek, M.; Xu, X.; Eckhold, P. et al. Substrate-induced magnetic ordering and switching of iron porphyrin molecules. *Nature Materials* **2007**, *6*, 516.

(7) Bernien, M.; Miguel, J.; Weis, C.; Ali, M.; Kurde, J.; Krumme, B.; Panchmatia, P.;

Sanyal, B.; Piantek, M.; Srivastava, P. et al. Tailoring the Nature of Magnetic Coupling of Fe-Porphyrin Molecules to Ferromagnetic Substrates. *Phys. Rev. Lett.* **2009**, *102*, 047202.

(8) Nakajima, A.; Kaya, K. A Novel Network Structure of Organometallic Clusters in the Gas Phase. *J. Phys. Chem. A* **2000**, *104*, 176–191.

(9) Atodiresei, N.; Dederichs, P. H.; Mokrousov, Y.; Bergqvist, L.; Bihlmayer, G.; Blügel, S. Controlling the Magnetization Direction in Molecules via Their Oxidation State. *Phys. Rev. Lett.* **2008**, *100*, 117207.

(10) Hosoya, N.; Takegami, R.; Suzumura, J.; Yada, K.; Miyajima, K.; Mitsui, M.; Knickelbein, M.; Yabushita, S.; Nakajima, A. Formation and Electronic Structures of Organoeuropium Sandwich Nanowires. *J. Phys. Chem. A* **2014**, *118*, 8298–8308.

(11) Tsuji, T.; Hosoya, N.; Fukazawa, S.; Sugiyama, R.; Iwasa, T.; Tsunoyama, H.; Hamaki, H.; Tokitoh, N.; Nakajima, A. Liquid-Phase Synthesis of Multidecker Organoeuropium Sandwich Complexes and Their Physical Properties. *J. Phys. Chem. C* **2014**, *118*, 5896–5907.

(12) Huttmann, F.; Schleheck, N.; Atodiresei, N.; Michely, T. On-Surface Synthesis of Sandwich Molecular Nanowires on Graphene. *J. Am. Chem. Soc.* **2017**, *139*, 9895–9900.

(13) Miyajima, K.; Yabushita, S.; Knickelbein, M.; Nakajima, A. Stern-Gerlach Experiments of One-Dimensional Metal-Benzene Sandwich Clusters: $M_n(C_6H_6)_m$ (M = Al, Sc, Ti, and V). *J. Am. Chem. Soc.* **2007**, *129*, 8473–8480.

(14) Zhang, X.; Ng, M.-F.; Wang, Y.; Wang, J.; Yang, S.-W. Theoretical Studies on Structural, Magnetic, and Spintronic Characteristics of Sandwiched Eu_nCot_{n+1} ($n = 1-4$) Clusters. *ACS Nano* **2009**, *3*, 2515–2522.

(15) Xu, K.; Huang, J.; Lei, S.; Su, H.; Boey, F.; Li, Q.; Yang, J. Efficient organometallic spin filter based on Europium-cyclooctatetraene wire. *J. Chem. Phys.* **2009**, *131*, 104704.

(16) Yao, X.; Yuan, S.; Wang, J. Theoretical Studies of Sandwich Molecular Wires with Europium and Boratacyclooctatetraene Ligand and the Structure on a H-Ge(001)-2x1 Surface. *J. Phys. Chem. C* **2016**, *120*, 7088–7093.

(17) van Gastel, R.; N'Diaye, A.; Wall, D.; Coraux, J.; Busse, C.; Buckanie, N.; Meyer zu Heringdorf, F.-J.; Horn von Hoegen, M.; Michely, T.; Poelsema, B. Selecting a single orientation for millimeter sized graphene sheets. *Appl. Phys. Lett.* **2009**, *95*, 121901.

(18) Wills, J.; Alouani, M.; Andersson, P.; Delin, A.; Eriksson, O.; Grechnev, A. *Full-Potential Electronic Structure Method, Energy and Force Calculations with Density Functional and Dynamical Mean Field Theory*; Springer Series in Solid-State Sciences; Springer-Verlag Berlin Heidelberg, **2010**; Vol. 167.

(19) Binder, K.; Heermann, D. *Monte Carlo Simulation in Statistical Physics*; An Introduction; Springer-Verlag Berlin Heidelberg, **2010**; Vol. 5.

(20) Skubic, B. *Spin Dynamics and Magnetic Multilayers*; Dissertation: Uppsala University, **2007**.

(21) Nolting, W. *Theoretical Physics 8, Statistical physics*; Springer International Publishing, **2018**.

(22) Uppsala University, Department of Physics and Astronomy, Uppsala Atomistic Spin Dynamics code. `http://physics.uu.se/uppasd`, Last accessed on 2018-11-06.

(23) Eriksson, O.; Bergman, A.; Bergqvist, L.; Hellsvik, J. *Atomistic Spin Dynamics: Foundations and Applications*; Oxford University Press, **2017**.

(24) Kurikawa, T.; Negishi, Y.; Hayakawa, F.; Nagao, S.; Miyajima, K.; Nakajima, A.; Kaya, K. Multiple-Decker Sandwich Complexes of Lanthanide-1,3,5,7-Cyclooctatetraene $[Ln_n(C_8H_8)_m]$ (Ln = Ce, Nd, Eu, Ho, and Yb); Localized Ionic Bonding Structure. *J. Am. Chem. Soc.* **1998**, *120*, 11766–11772.

(25) Thole, B.; van der Laan, G.; Fuggle, J.; Sawatzky, G.; Karnatak, R.; Esteva, J.-M. 3d x-ray-absorption lines and the $3d^9 4f^{n+1}$ multiplets of the lanthanides. *Phys. Rev. B* **1985**, *32*, 5107.

(26) Förster, D.; Klinkhammer, J.; Busse, C.; Altendorf, S.; Michely, T. Epitaxial europium oxide on Ni(100) with single-crystal quality. *Phys. Rev. B* **2011**, *83*, 045424.

(27) Schumacher, S.; Huttmann, F.; Petrović, M.; Witt, C.; Förster, D.; Vo-Van, C.; Coraux, J.; Martínez-Galera, A.; Sessi, V.; Vergara, I. et al. Europium underneath graphene on Ir(111): Intercalation mechanism, magnetism, and band structure. *Phys. Rev. B* **2014**, *90*, 235437.

(28) Carra, P.; Thole, B.; Altarelli, M.; Wang, X. X-ray circular dichroism and local magnetic fields. *Phys. Rev. Lett.* **1993**, *70*, 694.

(29) Kachkanov, V.; Wallace, M.; van der Laan, G.; Dhesi, S.; Cavill, S.; Fujiwara, Y.; O'Donnell, K. Induced magnetic moment of Eu3+ ions in GaN. *Sci. Rep.* **2012**, *2*, 969.

(30) Thole, B.; Carra, P.; Sette, F.; van der Laan, G. X-ray circular dichroism as a probe of orbital magnetization. *Phys. Rev. Lett.* **1992**, *68*, 1943.

(31) Lisi, S.; Gargiani, P.; Scardamaglia, M.; Brookes, N.; Sessi, V.; Mariani, C.; Betti, M. Graphene-Induced Magnetic Anisotropy of a Two-Dimensional Iron Phthalocyanine Network. *J. Phys. Chem. Lett.* **2015**, *6*, 1690–1695.

(32) Klinkhammer, J.; Förster, D.; Schumacher, S.; Oepen, H.; Michely, T.; Busse, C. Structure and magnetic properties of ultra thin textured EuO films on graphene. *Appl. Phys. Lett.* **2013**, *103*, 131601.

(33) Udvardi, L.; Szunyogh, L.; Palotas, K.; Weinberger, P. First-principles relativistic study of spin waves in thin magnetic films. *Phys. Rev. B* **2003**, *68*, 104436.